LAWRENCE
LIVERMORE
NATIONAL
LABORATORY

LLNL-JRNL-420171

The Advanced Helical Generator

D. B. Reisman, J. B. Javedani, G. F. Ellsworth, R. M. Kuklo, D. A. Goerz, A. D. White, L. J. Tallerico, D. A. Gidding, M. J. Murphy, J. B. Chase

November 12, 2009

Review of Scientific Instruments

Disclaimer

The Advanced Helical Generator

D.B. Reisman*, J.B. Javedani, G.F. Ellsworth, R.M. Kuklo, D.A. Goerz, A.D. White, L.J. Tallerico, D.A. Gidding, M.J. Murphy

Lawrence Livermore National Laboratory, Livermore, CA 94550

J.B. Chase

Jay B. Chase Consulting, Alameda, CA

Abstract

A high explosive pulsed power (HEPP) generator called the Advanced Helical Generator (AHG) has been designed, built, and successfully tested. The AHG incorporates design principles of voltage and current management to obtain a high current and energy gain. Its design was facilitated by the use of modern modeling tools as well as high precision manufacture. The result was a first-shot success. The AHG delivered 16 Mega-Amperes of current and 11 Mega-Joules of energy to a quasi-static 80 nH inductive load. A current gain of 154 times was obtained with a peak exponential rise time of 20 μs. We will describe in detail the design and testing of the AHG.

*E-mail: reisman1@llnl.gov

PACS numbers: 84.70.+p, 47.65.-d

Introduction

HEPP devices are based on the principle of the compression of magnetic fields by means of explosively driven metallic conductors. Invented by Andre Sakharov[1,2] (and independently by several others including Shearer[3] and Fowler[4]) in the 1950's, these devices have been used to reach energy and current outputs unobtainable by conventional

capacitor bank systems. These systems come in many forms, ranging from small flat plates to large disk and coaxial systems[5-8].

The generators work on the principle of conservation of flux Φ=LI, where L is inductance and I is current. Initially, current and thus flux is established across conductors. The detonation of the high explosive then compresses the conductors, resulting in a rapid decrease in inductance. To conserve flux, the current correspondingly rises with decreasing inductance. If we neglect losses, the final amplification of current is then simply proportional to the ratio of final to initial inductance.

$$I_f = I_0 \frac{L_0}{L_f} \quad (1)$$

Helical generators work on the principal of the moving short circuit. These systems consist of an explosive packed metal cylinder placed inside a helical coil. The cylinder is detonated at one end. The moving metal cylinder is referred to as the armature whereas the coil it contacts is referred to as the stator. As the explosively driven cylinder expands it makes contact with the helical coil. This moving, rotating short circuit reduces the inductance of the system as the expanding armature cone moves from one end of the generator to the other (Figure 1).

In practice, helical generators do not exactly conserve flux. Due primarily to the high electrical resistance encountered as the armature contacts the coil and magnetic fields are enhanced to Mega-Gauss levels, a fraction of flux leaves the system. Empirically this can be described by the formula

$$L\dot{I} + \alpha \dot{L} I = 0 \quad (2)$$

This formula simply states that the generator will lose a fraction of 1-α of flux for every e-folding of current.

Integrating we obtain

$$I = I_0\left(\frac{L_0}{L}\right)^{\alpha} \quad (3)$$

Generally α varies between 0.7-0.9 for most large, Mega-Ampere systems. In our experience, proper management of voltage and current will result in an α of 0.88.

Voltage and current management are of great importance to helical generator design. We can express the peak internal voltage as

$$V_I = \dot{L}I \quad (4)$$

Through experiment it has been found that generators begin to experience breakdowns at about 160 kV. Like any empirical rule this is probably specific to the classes of generators considered in this paper and is open to debate.

Good generator design should strive to keep V_I within some narrow range during the operation and not exceed the empirical threshold. If we combine equations (2) and (4), insisting on constant V_I, we obtain a formula for the time dependent inductance of the generator.

$$L(t) = \left[\frac{(\alpha-1)V_I t}{I_0(L_0+L_s)^{\alpha}} + \frac{1}{(L_0+L_s)^{\alpha-1}}\right]^{\frac{1}{1-\alpha}} - L_s \quad (5)$$

I_0 is the initial seed current of the generator and L_S is the inductance of the static load attached to the generator.

The inductance as a function of armature-stator contact position, x, can be expressed as

$$L(x) = L\left(t \to \frac{x}{v_{DET}} \right) \quad (6)$$

V_{DET} is the explosive detonation velocity and thus the velocity of the moving contact point along the axis of the generator.

Given the radius of the stator coil and explosive armature, the generator can then be fully described using the turn density

$$n(x) = \sqrt{\frac{\frac{dL}{dx}}{4\pi^2\left(R^2_{STAT} - R^2_{ARM}\right)}} \quad (7)$$

Equation (7) is based on the infinite length sheet current model for inductance and thus does not include three-dimensional effects. It does serve as a good approximation to turn density. We will describe a more accurate model in the next section that is used to determine the final design.

The management of current density is also of great concern in the design of helical generators. Experimentally it has been found that if linear current density exceeds 0.4 MA/cm, resistive losses will dominate. The result will be a generator that loses most of its flux and does not have sufficient energy and current gain. Early generator designs suffered from this effect, losing 75% of their initial flux during operation[3].

In order to manage the losses encountered from high current density, most generator designs use the bifurcation of coils. Typically, the generator is divided up into sections. Between adjacent sections a transition is made and the number of parallel coils is doubled. Therefore, as the generator operates the current per wire will be reduced by a factor of two at each section transition.

I. AHG DESIGN

The requirements of the AHG were to produce approximately 20 MA of current into a 80 nH load with a final exponential rise time of 20 ms. The initial seed current was to be provided by a 300 kJ capacitor bank. The output requirement coupled with the input current determines the parameters of the design. These were chosen as

L_0=27 μH

I_0=120 kA

We chose to divide the generator into 5 sections of different pitch. Note that in order to obtain nearly constant V_I our pitch must increase with length. The generator was bifurcated at 4 sections. In the first two sections, 2 wires are wound in parallel. The third, fourth, and fifth coils sections have 4, 8, and 16 wires in parallel, respectively. The winding sections, pitch, and number of parallel wires is shown in Figure 3 .

To accommodate the 27 μH inductance, we chose an armature radius of 15.25 cm and a stator coil radius of 24.5 cm. The total coil length was determined from equation (6) to be 1 meter. The armature is 1.9 cm thick 6061 fully annealed aluminum. The expansion ratio of the armature is 1.6. It has been found experimentally that aluminum armatures have good integrity up to an expansion of 1.75 time initial diameter.

A constant copper wire diameter of 0.9525 cm (3/8 inch) was used in the generator. A wire filling fraction (center-to-center wire spacing divided into the diameter of the wire) of between 0.6-0.7 was maintained throughout.

The explosive armature was filled with 159 kg of PBXN-110 cast explosive. This specific explosive has a detonation speed of v_{DET}=0.79 cm/μs and an energy density of 0.088 MJ/cm^3. The armature expansion angle was calculated to be 15 degrees. The

explosive package also incorporates a 10 cm diameter plane wave lens to initiate the main PBXN-110 cylinder. The full AHG device is shown in Figure 2.

The stator coil was wound on a collapsible grooved mandrel (Figure 4). The grooves are machined to a depth of 20% of wire diameter. This greatly facilitated the winding and allowed strict tolerances (<0.05 cm) on wire spacing and radius. After winding, the assembly was potted in epoxy through a vacuum fill process. The epoxy as well as a G10 outer sleeve provided structural stability. After the epoxy is cured, the inner mandrel is removed.

II. Simulation

Although the formulas derived in the last section provide some guidance for design, a more accurate dynamical model is needed. A computer model was used to predict AHG performance as well as refine the initial design. The model code CAGEN[10] was used for this purpose. CAGEN is a dynamic, self-consistent helical generator model. CAGEN solves the common circuit model for the generator

$$\frac{d}{dt}\left(L_i I_i\right) + R_i I_i = 0 \quad (8)$$

The motion of the armature is calculated separately with a hydrodynamic code and input in tabular form. Variable coil pitch and bifurcations are represented and used to calculate inductance. The magnetohydrodynamic equations are used to calculate the effect of the magnetic fields on the conductors. The resistance, melting, flux loss, pressure and contact effects are calculated. Of primary importance is the contact resistance[11] that is affected by the proximity of the armature to the stator coil. The region around the armature-stator contact point will heat to such an extreme that non-linear

magnetic diffusion will dominate. Flux will therefore leak out of the generator through the region near that point.

The CAGEN model has been used to model a variety of generators[12]. For our purposes, CAGEN was used iteratively to refine the design. An initial inductance and current was first determined that would give the desired final current into a specific inductance. Then an inductance and winding density was estimated using equations (5) and (7).

The winding was broken up in several constant pinch sections that would approximate the desired winding density. Locations for the bifurcations were also chosen at this time. After inputting these parameters, the section pitches were further refined to obtain a nearly constant internal voltage.

The final design current, inductance, and internal voltage were calculated. The predicted current reaches a maximum of 20 MA with a seed current of 120 kA (Figure 5). This implies a gain of 170 and a current alpha of 0.91. The internal voltage is shown in Figure 6. Although it slightly dips at each bifurcation transition, it dos not exceed 140 kV, well within our empirical limit. The inductance is shown in Figure 7. It exhibits an exponential decay like behavior from in initial value of approximately 27.25 μH.

III. Hydrodynamic modeling and Design

Several aspects of the AHG design were aided by hydrodynamic modeling. As mentioned above, the armature expansion acceleration profile is used in CAGEN calculations. This was computed with the two-dimensional arbitrary Lagrangian-Eulerian hydrodynamic code CALE[13]. The JWL equation of state (EOS) for PBXN-112 was used

with a programmed burn velocity. An EOS and constitutive model for strength was used for the aluminum armature. The position and velocity versus time is shown in Figure 8.

Of critical importance is the design of the crowbar region of the helical generator. As the coil is seeded with current from the capacitor bank, the explosive is detonated at a predetermined time. This time is chosen so that crowbar occurs when the seed current reaches peak value. Special care must be taken not to disrupt the flow of current before crowbar time with the explosive action of expansion at the input end of the generator. Also, the crowbar must be designed so that it makes good contact with the armature and creates a smooth transition for the armature as it approaches the first winding section.

A calculation was set up to simulate the hydrodynamics of the AHG (Figure 9). This calculation included the explosive armature as well the metal flanges and crowbar region of the generator. Through calculation it was determined that a high density metal should be used as the crowbar material. Specifically, the design uses two angled pieces of tungsten each with a width of 10 cm. Figure 10 shows the crowbar action and the sliding interface created by the contact of the aluminum armature against the tungsten crowbar. These calculations were performed in two dimensions and therefore assumed that the crowbar was a cylindrically symmetric object. They nevertheless guided the final design.

Hydro calculations were also used to design the “output cone” of the generator. As the armature passes the last winding it mates with an angled cone of slightly larger angle (Figure 11). The function of the output cone is to minimize final inductance and thus maximize current and flux delivery to the load.

IV. Electromagnetic Calculations and Insulator Power-Flow Design

The management of electrical fields and voltages is of key importance to HEPP design. Voltage breakdown losses must be avoided in order to obtain the required current and energy gain. Electrical field management is important in several places in the device. The first area is at the input end where the seed bank cables connect to the generator. Here proper stand-off distances must be maintained to avoid flashover at the cable breakout point. The second area is, as mentioned before, between the armature and the helical coils. In addition to not exceeding the critical internal voltage V_I, other measures are taken to prevent breakdown. The generator is filled with SF6, an electronegative gas, which has a higher breakdown threshold than air. SF6 breaks down at 75 kV/cm whereas air breaks down at only 25 kV/cm. Further insulation is provided by wrapping the inner diameter of the coil with 4 layers of 0.0127 cm thick Mylar sheet. The use of Mylar wrapping and SF6 is common practice in helical generator design[9,15-17].

The third area where electrical field management is critical is at the interface between the AHG and the load. This interface consists of a layer of polyethylene that extends from the inner wall of the output cone, through a narrow (1 cm thick) cylindrical section, and then radially outward where it terminates at the input of the inductive load (Figure 13). To avoid electrical breakdown, care must be taken not to exceed the breakdown threshold at several points. One of these areas is the triple point where metal, gas, and plastic insulator intersect. Another area is in the insulator region between the metal conductors.

Detailed electrostatic calculations are used to investigate the various regions. First an estimate of peak voltage is made using CAGEN. Then Maxwell 2D[18], an electrostatic finite element code, is used to calculate the electrical filed throughout the entire

geometry. A line-out plot of the electrical field taken around the power-flow region is shown in Figure 14. The minimum threshold for breakdown, which is the maximum field that can be held off by SF6 gas at STP, is also shown. Because the electrical field stays below this threshold, the integrity of the power-flow region can be maintained. In practice, calculations of this type are used to refine the design so that inductance is minimized in the power-flow region while good electrical properties are maintained.

V. Experiment

The AHG experiment was conducted at the Big Explosive Experimental Facility (BEEF) at the Nevada Test Site. BEEF is a bunker facility capable of firing thousands of pounds of high explosives. Experiments are conducted on top of the shielded bunker. The device is placed on the shot table around which are placed blast enclosures which contain auxiliary systems such as firesets, pressured gases, and the seed bank (Figure 15). Inside the bunker are located control systems that fire the experiment and data collection systems that record experimental data. Data is transmitted via fiber or shielded cable to digitizers inside of the bunker.

For purposes of testing, the AHG was attached to a quasi-static 80 nH inductive load (Figure 2). The distinction is made for quasi-static since the large magnetic pressures in the load causes some change in inductance near peak current. To fully diagnose current delivery, diagnostics were places at every stage of the experiment. Pearson current probes were used to measure output from the seed bank. Inductive loop (Bdot) current probes were placed in the load region as well as in the insulator region between the AHG output cone and load. Rogowski loops and optical fiber Faraday rotation sensors were also placed inside the load.

The AHG was seeded with a 1.33 mF capacitor back located in an adjacent blast enclosure. The current was transported along four DS2248 cables to the experiment. A peak current of 100 kA was obtained with a quarter sine wave rise time of approximately 300 μs (Figure 16).

Approximately 16 MA of current were delivered to the load with an exponential rise time of 20 μs (Figure 17). Each of the Bdot and Rogowski loop currents are the result of averaging two opposite polarity probes. This is done to subtract out any common mode noise. The input Bdots recorded higher peak current (16.4 MA) than the output Bdot (15.5 MA). The peak Faraday (15.6 MA) and Rogowskii (16.0 MA) currents were both below that of the Bdots. We have the highest confidence in the output Bdots as those probes were calibrated *in situ* with a network analyzer technique. Furthermore, since the output Bdot probes were electrically shielded by the use of a Faraday cage they encountered almost no common mode signal.

VI. Code Comparison

Calculations were performed with CAGEN and compared to the experimental results (Figures. 18 and 19). Excellent agreement was obtained in Idot and current. The calculation included the transition to the output cone as well as a one-dimensional model for the quasi-static load dynamics that undergoes some collapse along the inner cylinder.

To obtain a better estimate of peak flux, magnetic energy and integrated electrical energy, magnetohydrodynamic calculations were performed. Again the code CALE was used with a toroidal magnetic field and a full EOS, strength, and resistivity model for the aluminum conductors.

The load was simulated in two dimensions with an input current from the experiment. It was seen that significant collapse of the inner liner occurs near peak current. By the time of peak current the central radius of the inner coax of the load has decreased to a radius of 7.9 cm from an initial radius of 8.4 cm. Due to this change the inductance of the 80 nH load increases to 88 nH at the time of peak current. Using these calculations we obtained a maximum flux of 15 MG cm^2. We also obtain a peak magnetic energy of 10 MJ with an integrated electrical energy of 11 MJ (Figure 20).

VII. Application

The AHG was designed to provide the seed current for a coaxial generator (COAX) of similar inductance of that of the quasi-static load discussed above. Three experiments of this type were performed. Each experiment was seeded with 110 kA. The peak outputs current of the AHG for all of these experiments was 17 MA (Figure 21). The details of the full integrated design consisting of AHG and COAX and the experimental results will be discussed in future publications.

VIII. Conclusion

We have developed a high-gain HEPP generator, the AHG. The design of the AHG was aided by the use of modern design tools such as the helical design code CAGEN, the magnetohydrodynamic code CALE, and the electrostatic code Maxwell 2D. Precision fabrication techniques were used to maintain tight tolerances required for proper operation. The AHG was successfully tested and resulted in a current delivery of 16 MA to an 80 nH quasi-static inductive load. Approximately 11 MJ of integrated electrical energy was delivered. The comparison between the data and simulation is good and validates the detailed modeling approach taken in the development of the AHG.

Acknowledgements

The authors would like to thank the support of Bruce Goodwin and Charlie Verdon. The authors would also like to acknowledge program manager Scott McAllister. This work performed under the auspices of the U.S. Department of Energy by Lawrence Livermore National Laboratory under Contract DE-AC52-07NA27344.

References

1) A.D. Sakharov et al., Sov. Phys.-Doklady 10, 1045 (1966).

2) A.D. Sakharov, Sov. Phys.-Usp. 9,294 (1966).

3) J.W. Shearer *et al.*, **39**, 2102 (1960).

4) C.M. Fowler, W.B. Garn, and R.S. Caird, J. Appl. Phys. **31**, 588 (1960).

5) A.I. Pavlovskii, et al., in *Megagauss Physics and Technology*, edited by P.J. Turchi, (Plenum Press, New York, 1980), p. 585.

6) V.K. Chernyshev et al, in *Digest of Technical Papers, Eighth IEEE Pulsed Power Conference*, edited by K. Prestwich and R. White, (IEEE, New York, 1991), p. 419.

7) Magnetocumulative Generators, Larry L. Altgilbers et al., (Springer-Verlag New York, 2000).

8) Explosively Driven Pulsed Power, edited by Andreas A, Neuber, (Springer-Verlag, Berlin, 2005).

9) J.V. Parker, et al., in *Megagauss Magnetic Fields and High Energy Liner Technology*, edited by G.F. Kiuttu, P.J. Turchi, R.E. Reinovsky, (IEEE, New York, 2007), p. 265.

10) J.B. Chase, et al., in *Proceedings of 12th IEEE pulsed Power Conference*, (IEEE, New York, 1999), p. 597.

11) G.F. Kiutu, J.B. Chase, D.M. Chato, G. Peterson, in *Eighth Annual Directed Energy Symposium*, (2005).

12) J.B. Chase et al., *Megagauss XI*, edited by I. Smith and B. Novac, (The Institute of Engineering and Technology, London, 2007) , p. 99.

13) Tipton, R.E., in *Proceedings of the 4th International Conference on Megagauss Magnetic Field Generation and Related Topics*, edited by C.M. Fowler, R.S. Caird, and D.J. Erickson, (Plenum Press, New York, 1987), p. 299.

14) D.B. Hopkins, in *Engineering Problems of Fusion Research*, *Symposium on Engineering Problems of Fusion Research, 6th* , (IEEE, New York, 1976), p. 235.

15) Fowler, C.M., et al., *Digest of Papers, Seventh IEEE Pulsed Power Conference*, (IEEE, New York, 1989), p. 475.

16) E. Cnare and M. Cowan, in *Proceedings of the 5th IEEE Pulsed Power Conference*, edited by M.F. Rose and P.J. Turchi, (IEEE, New York, 1985), p. 194.

17) J.H. Degnan et al., *Ultra High Magnetic Fields – Physics, Techniques, Applications, Proceedings of the Third International Conference on Megagauss Magnetic Field Generation and Related Topics*, edited by V.M. Titov and G.A. Shvetsov, (Nauka, Moscow, 1983), p. 352.

18) © 2009 Ansoft, LLC.

Figure Captions

Figure 1: Operation of a helical high explosive pulsed power device.

Figure 2: Cutaway view of the AHG device.

Figure 3: Winding pattern of AHG.

Figure 4: AHG coil on grooved mandrel.

Figure 5: Current versus time.

Figure 6: Internal voltage versus time.

Figure 7: Inductance versus time.

Figure 8: Aluminum armature position and velocity versus time.

Figure 9: Calculation setup for AHG hydro simulation in CALE.

Figure 10: Armature-crowbar hydro images.

Figure 11: Hydrodynamic calculation showing armature mating with output cone.

Figure 12: Load voltage versus time.

Figure 13: Calculation setup in Maxwell2D for output cone to dummy load interface.

Figure 14: Calculation of electrical field in interface region. Electrical field does not exceed breakdown threshold for SF6 gas.

Figure 15: AHG generator shown on shot table at BEEF facility at NTS.

Figure 16: Current versus time from seed capacitor bank.

Figure 17: Current versus time for AHG. Shown are signal measured with output Bdots (IBDOTO), input Bdots (IBDOTI), Rogowskii coil (IROGO), and Faraday fiber probes (FARADAY).

Figure 18: Experimental current compared to CAGEN calculation.

Figure 19: Experimental current derivative (Idot) compared to CAGEN calculation.

Figure 20: Flux, magnetic energy, and integrated electrical energy delivered to load.

Figure 21: Current vs. time coupled AHG-coaxial generator experiments FFT1, FFT2, and FFT3.

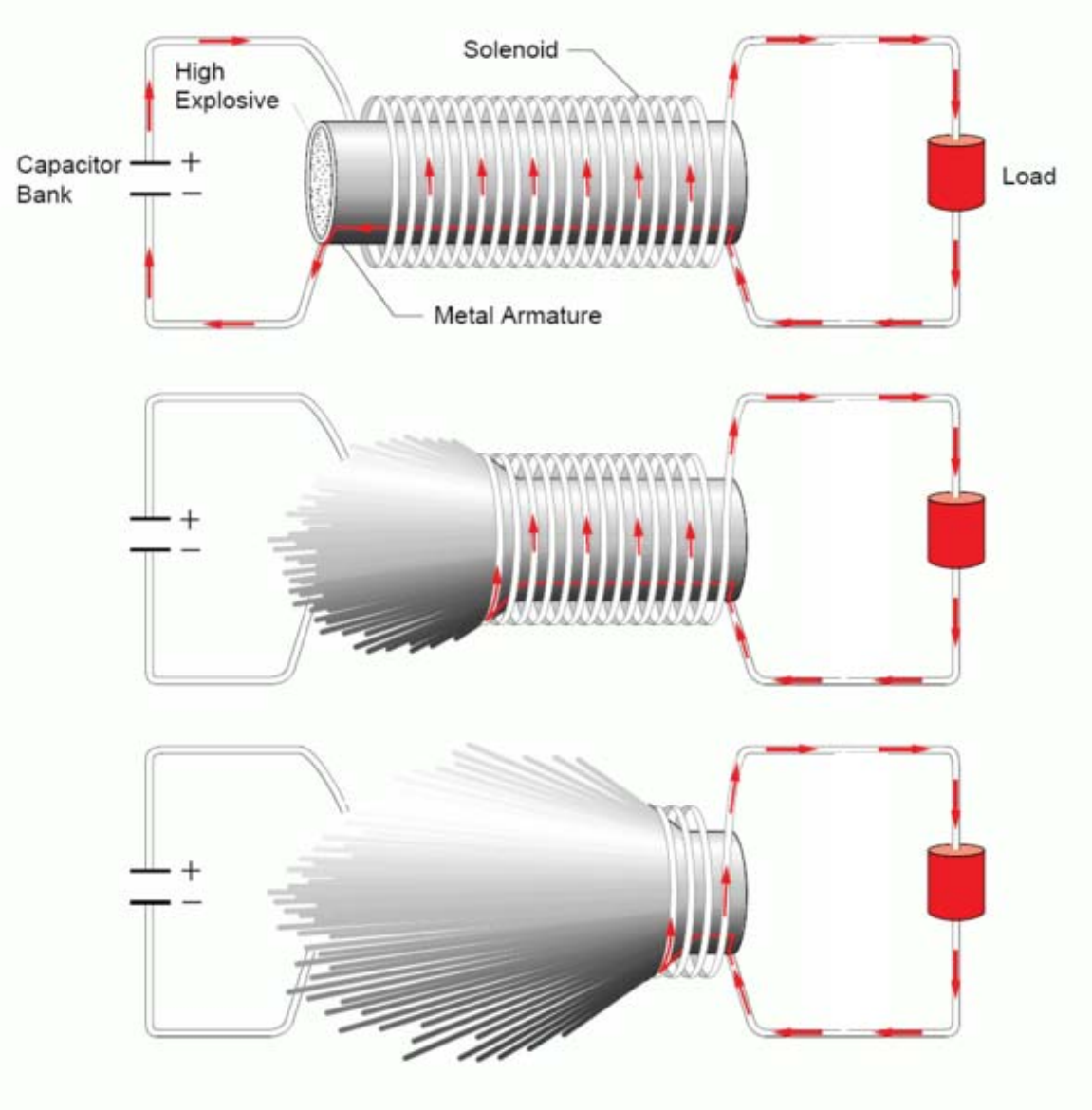
Solenoid
High
Explosive
Capacitor
Bank
+
−
Load
Metal Armature
+
−
+
−

Figure 1

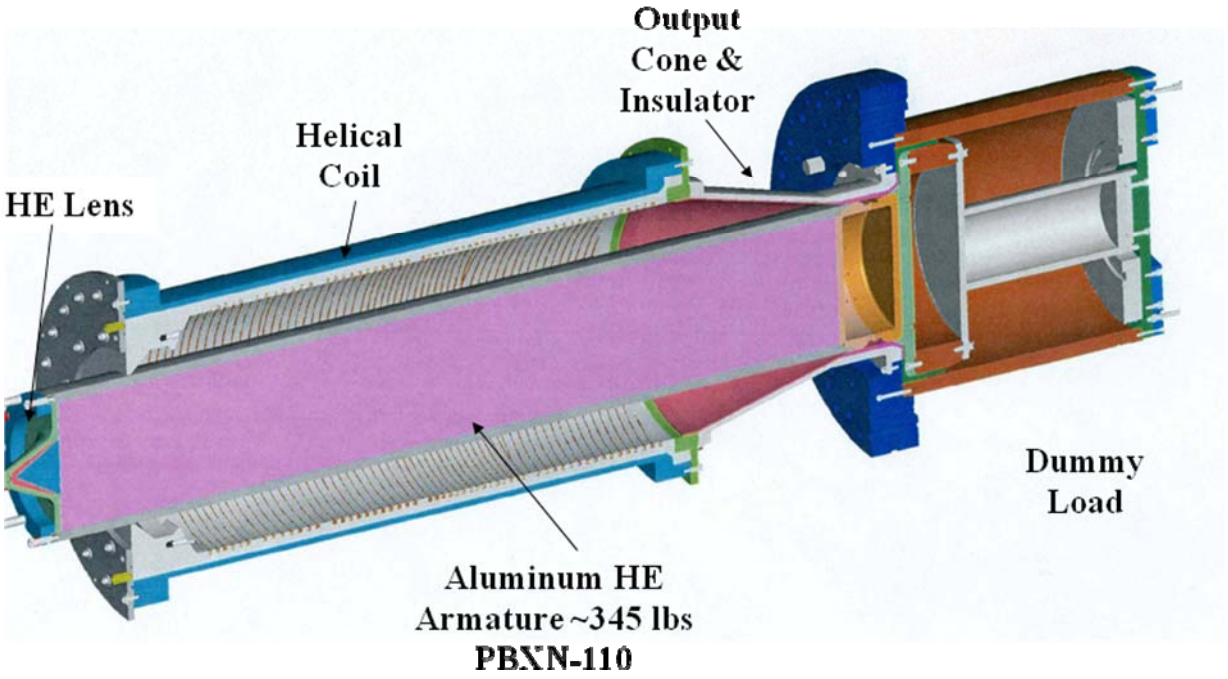
Output
Cone &
Insulator
Helical
Coil
HE Lens
Dummy
Load
Aluminum HE
Armature ~345 lbs
PBXN-110

Figure 2

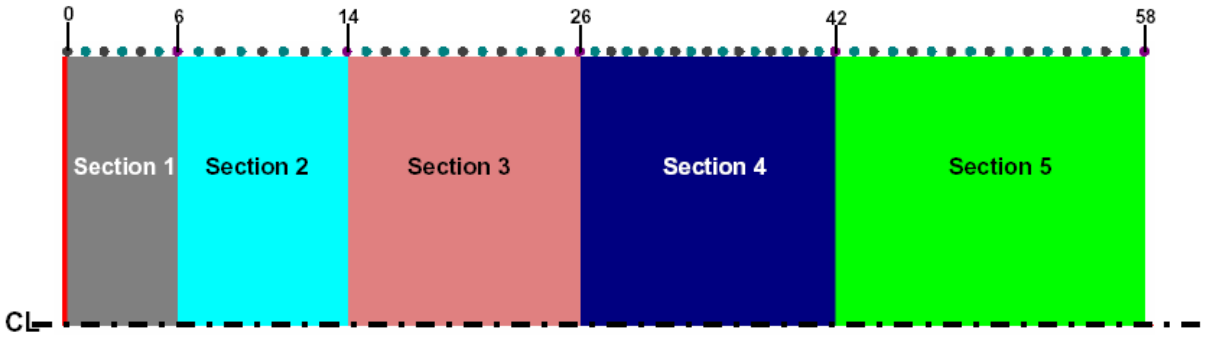

Section #	Length "cm"	Wire Spacing "cm"	Pitch "cm"	No of Turns	No of Wires in parallel	Wire Number
1	9.990	1.663	3.330	3	2	0-6
2	15.392	1.925	3.848	4	2	6-14
3	21.054	1.376	7.018	3	4	14-26
4	23.195	1.466	11.598	2	8	26-42
5	28.070	1.748	28.070	1	16	42-58

Figure 3

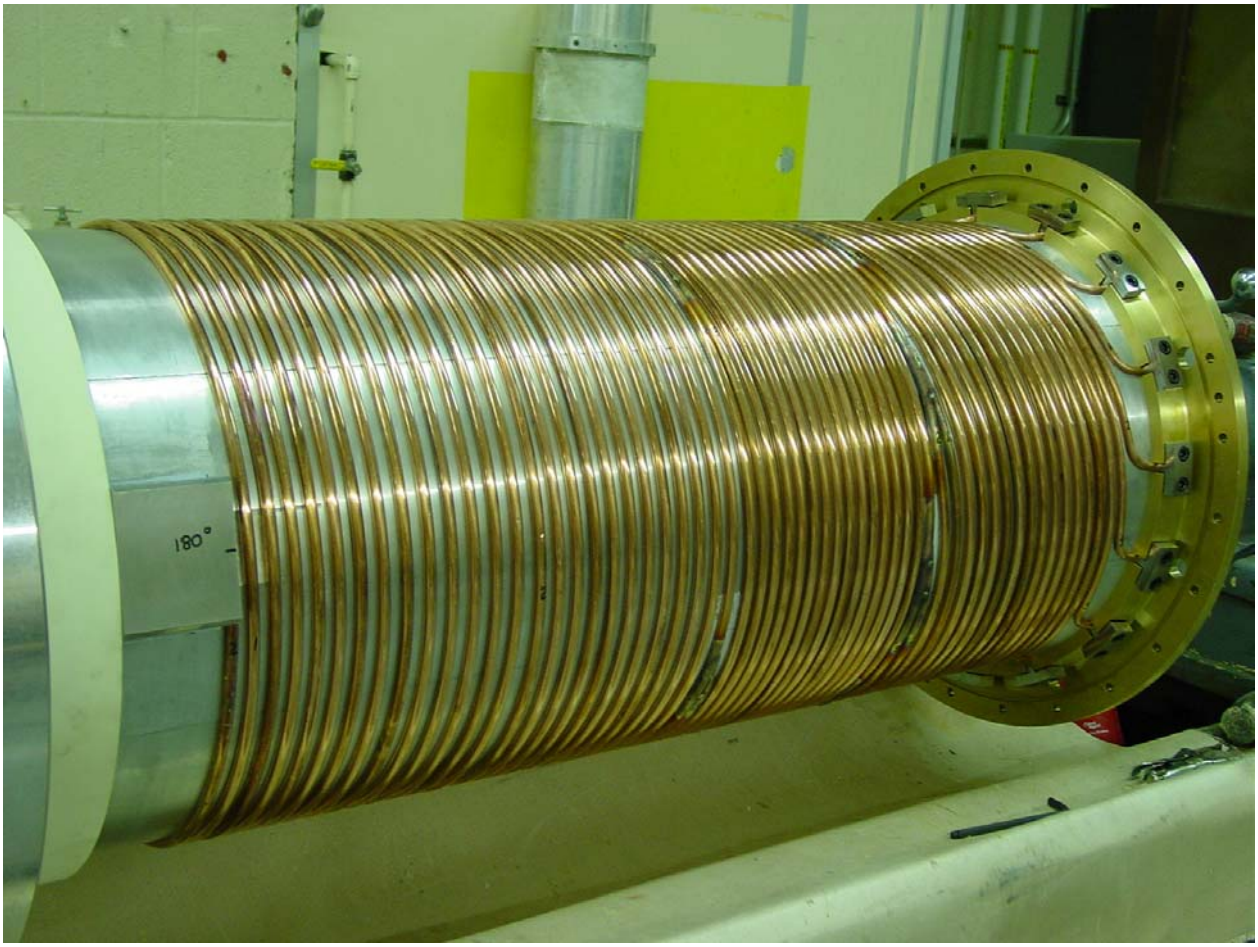

Figure 4

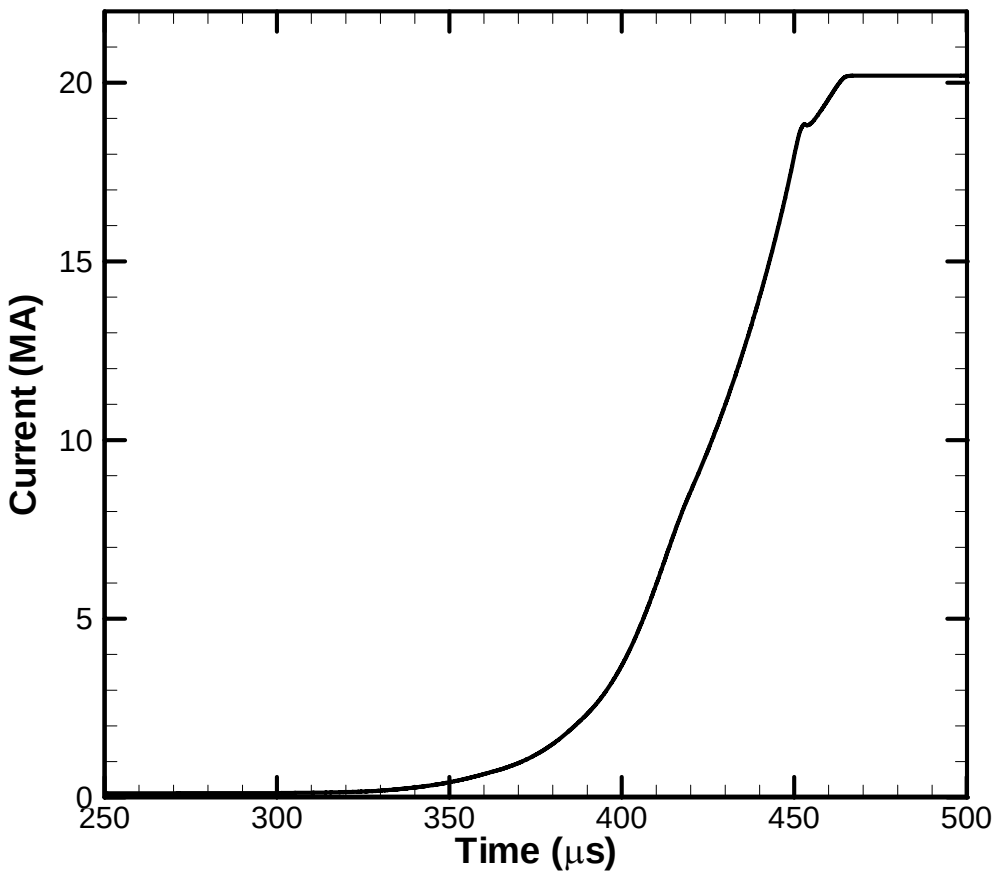

Figure 5

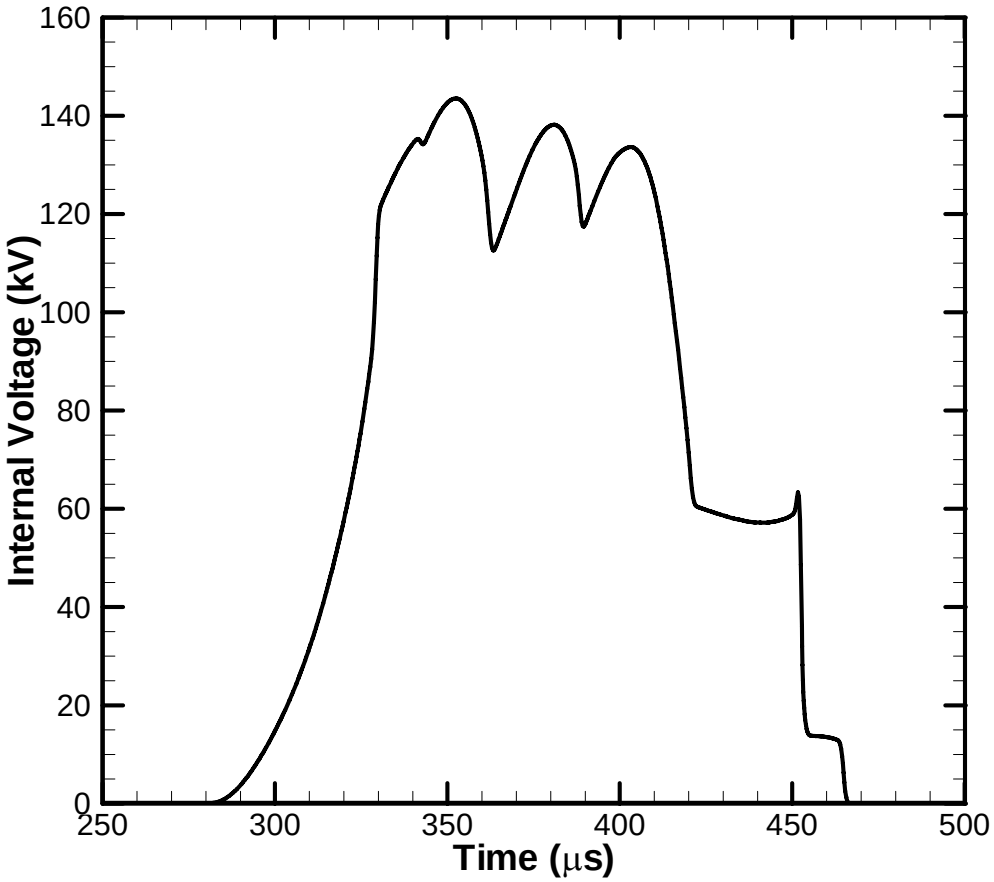
Internal Voltage (kV)
160
140
120
100
80
60
40
20
0
250
300
350
400
450
500
Time (μs)

Figure 6

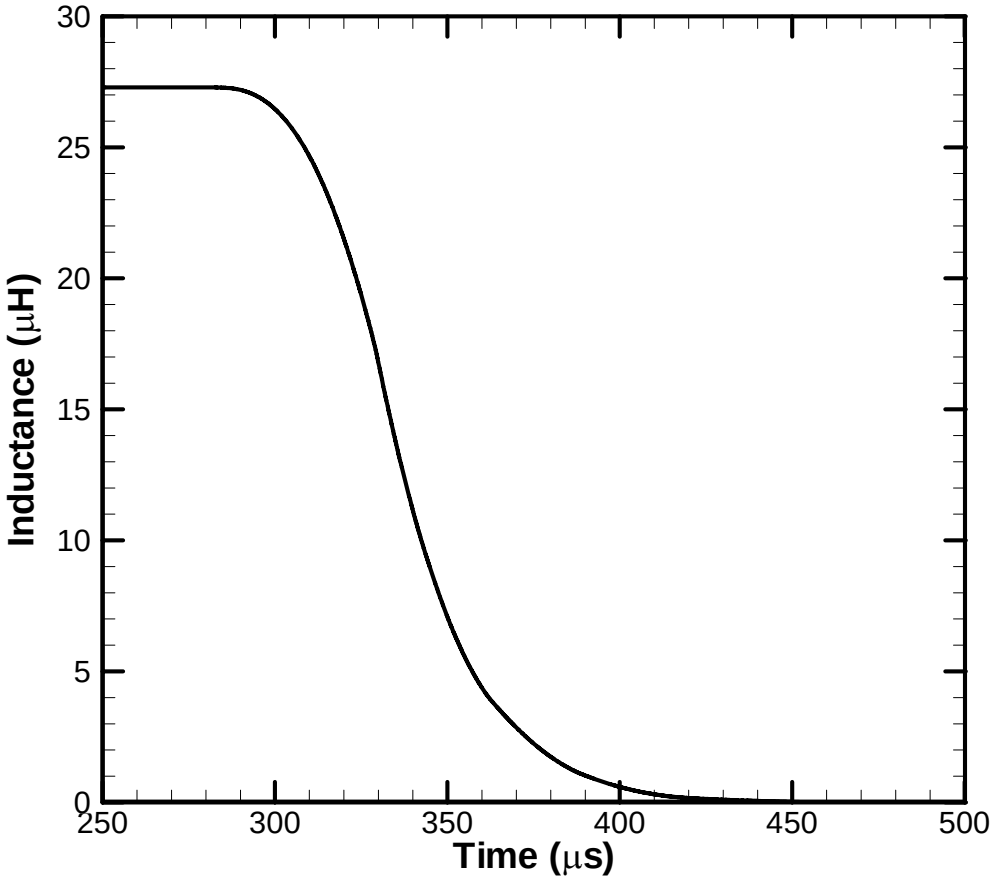

Figure 7

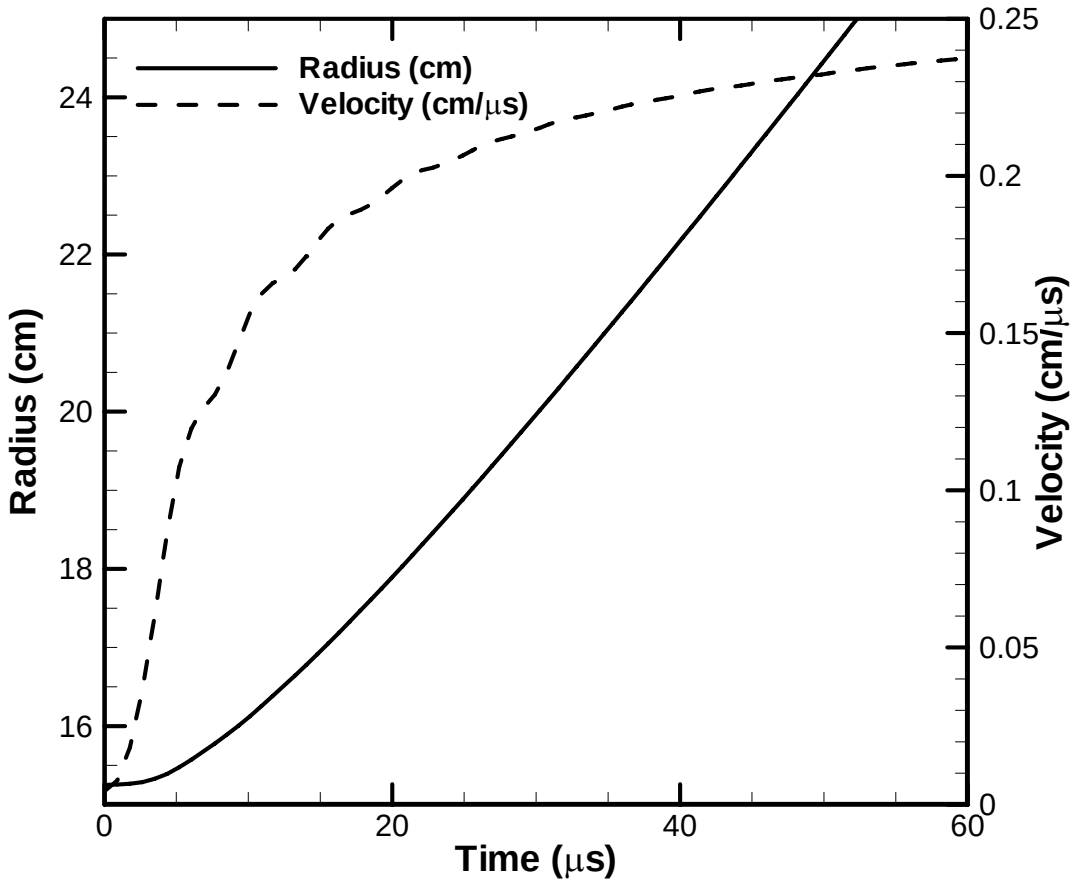
Radius (cm)
Velocity (cm/μs)
Radius (cm)
Velocity (cm/μs)
Time (μs)
16
18
20
22
24
0
0.05
0.1
0.15
0.2
0.25
0
20
40
60

Figure 8

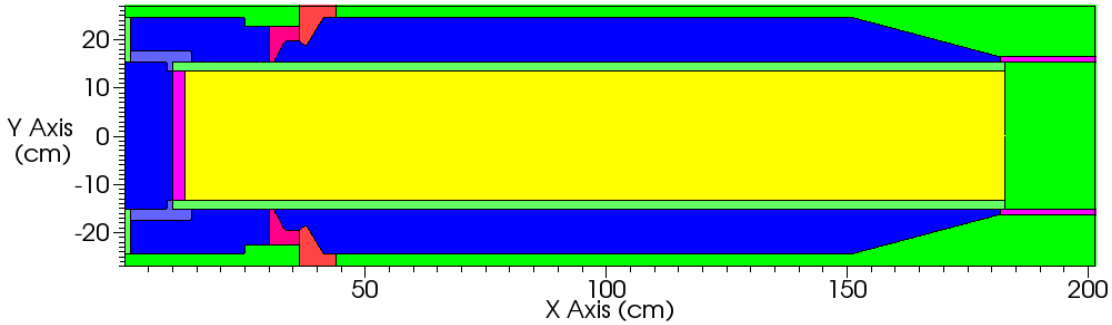

Figure 9

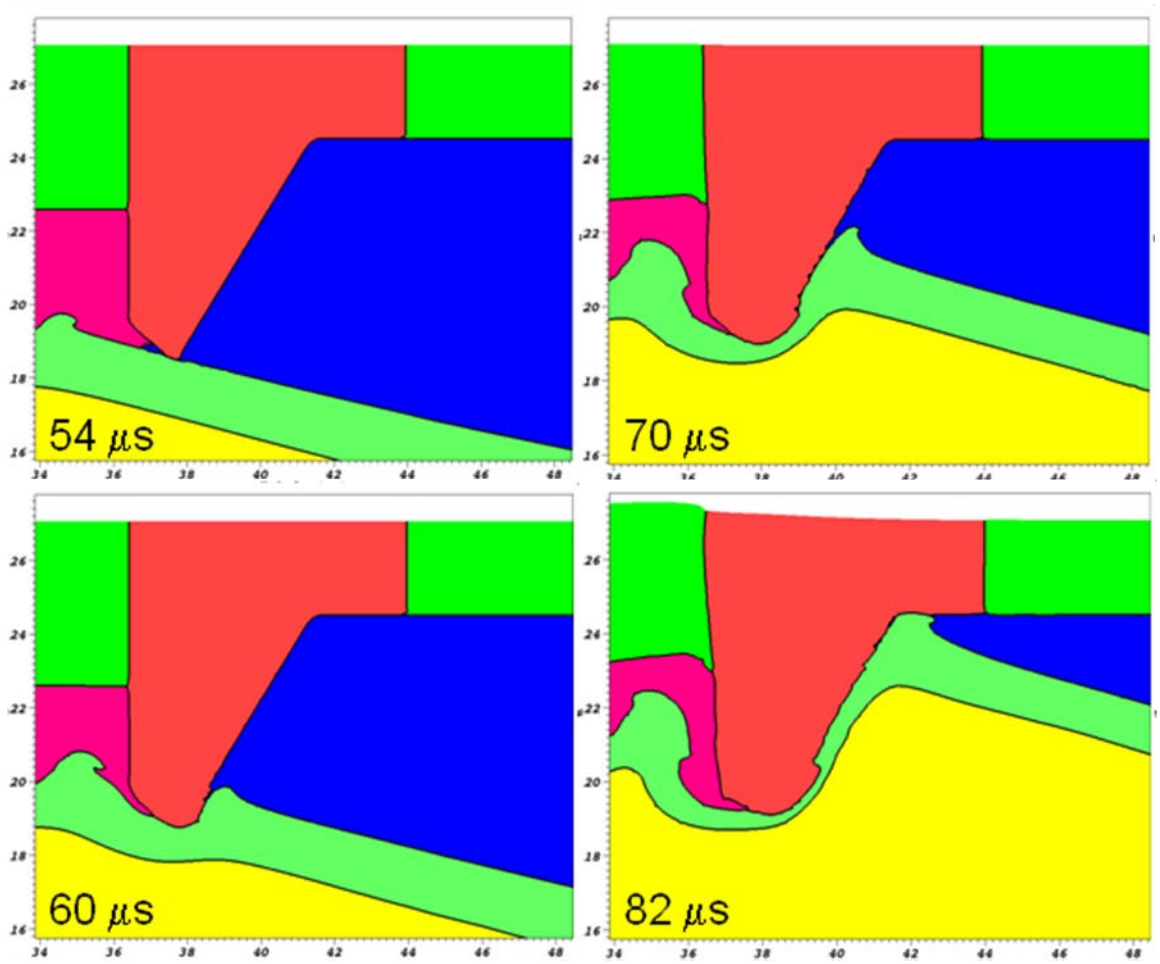

Figure 10

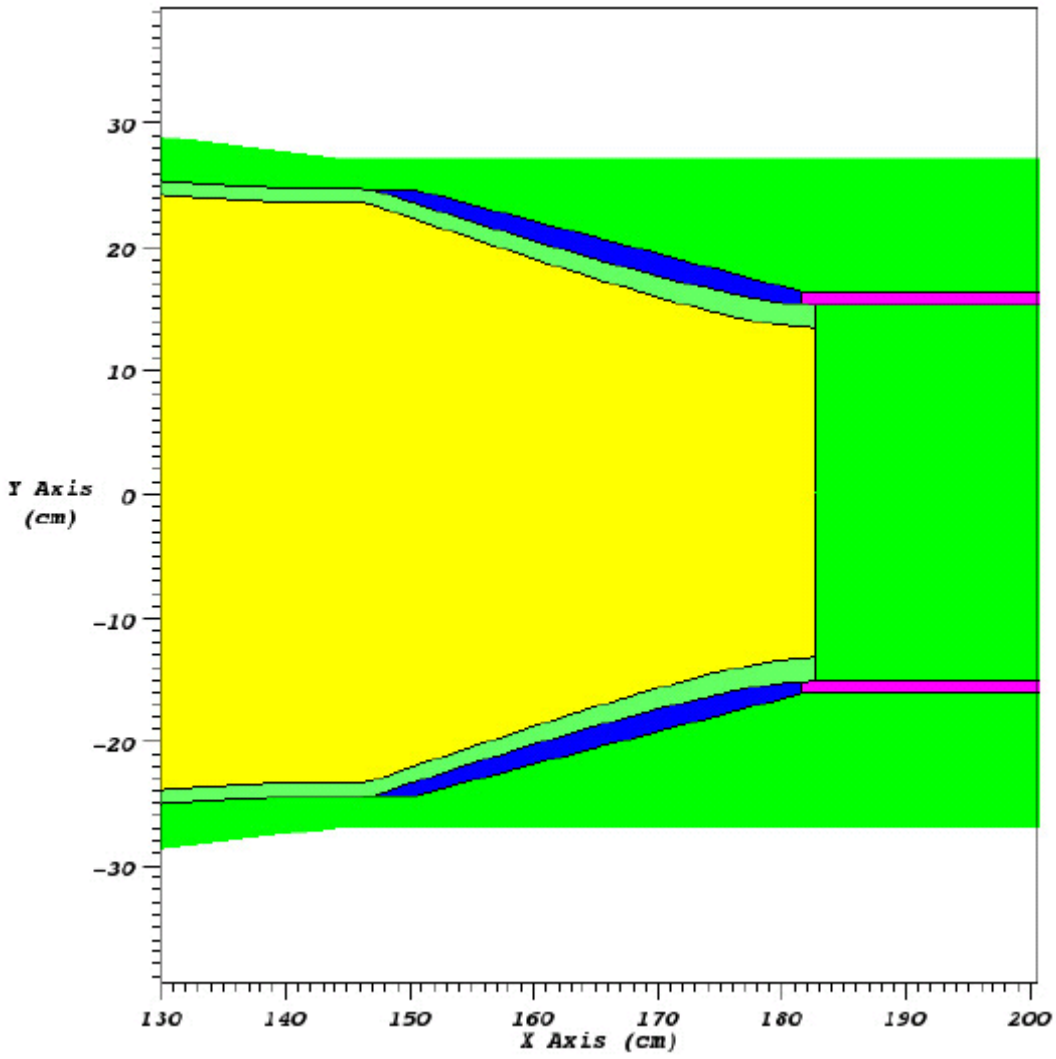
30
20
10
0
-10
-20
-30
Y Axis
(cm)
130
140
150
160
170
180
190
200
X Axis (cm)

Figure 11

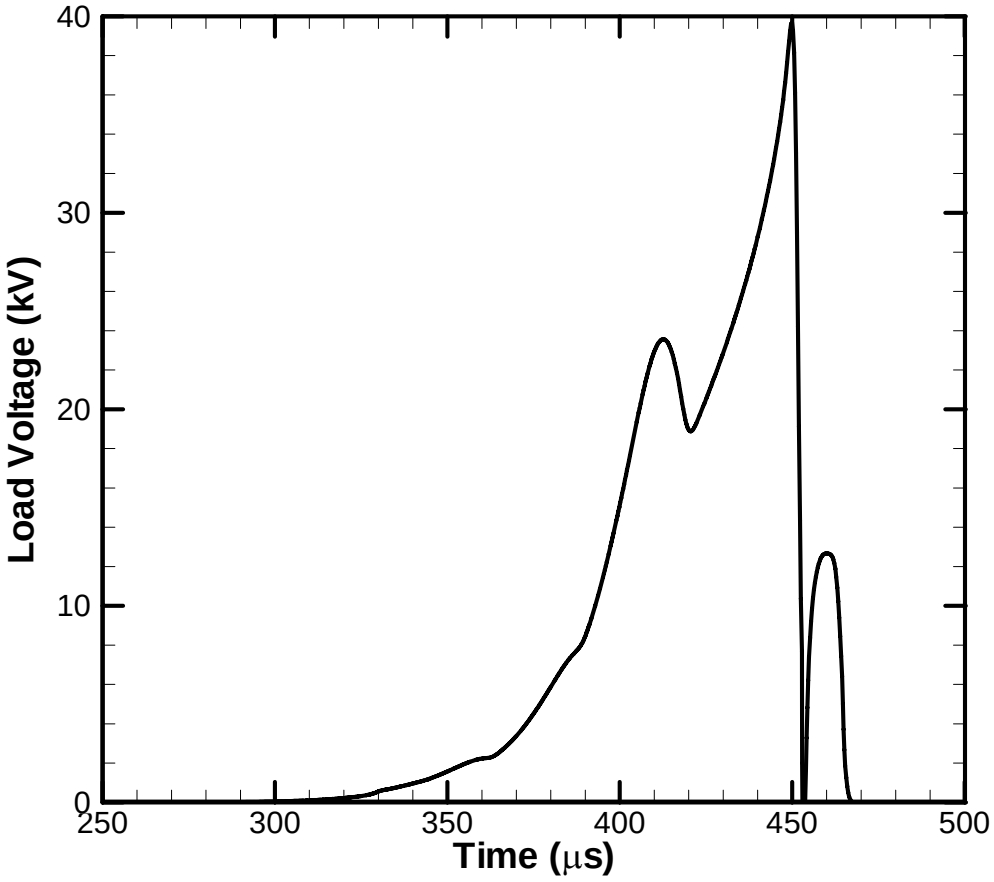

Figure 12

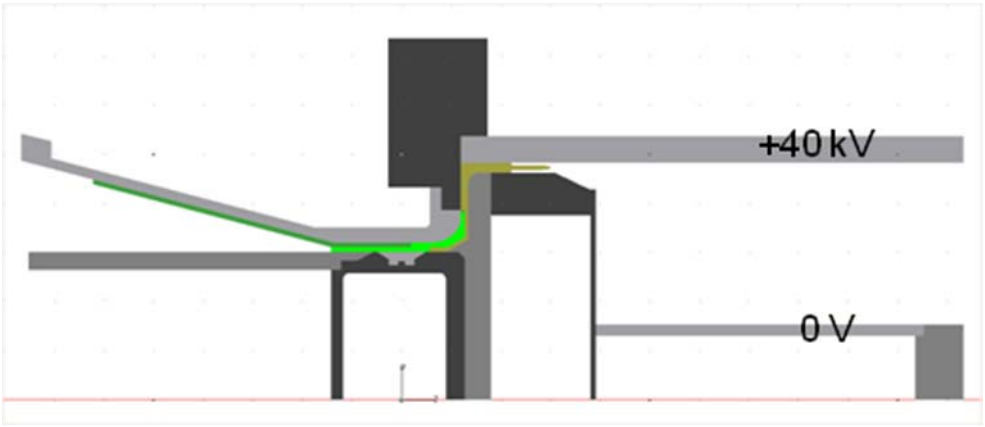

Figure 13

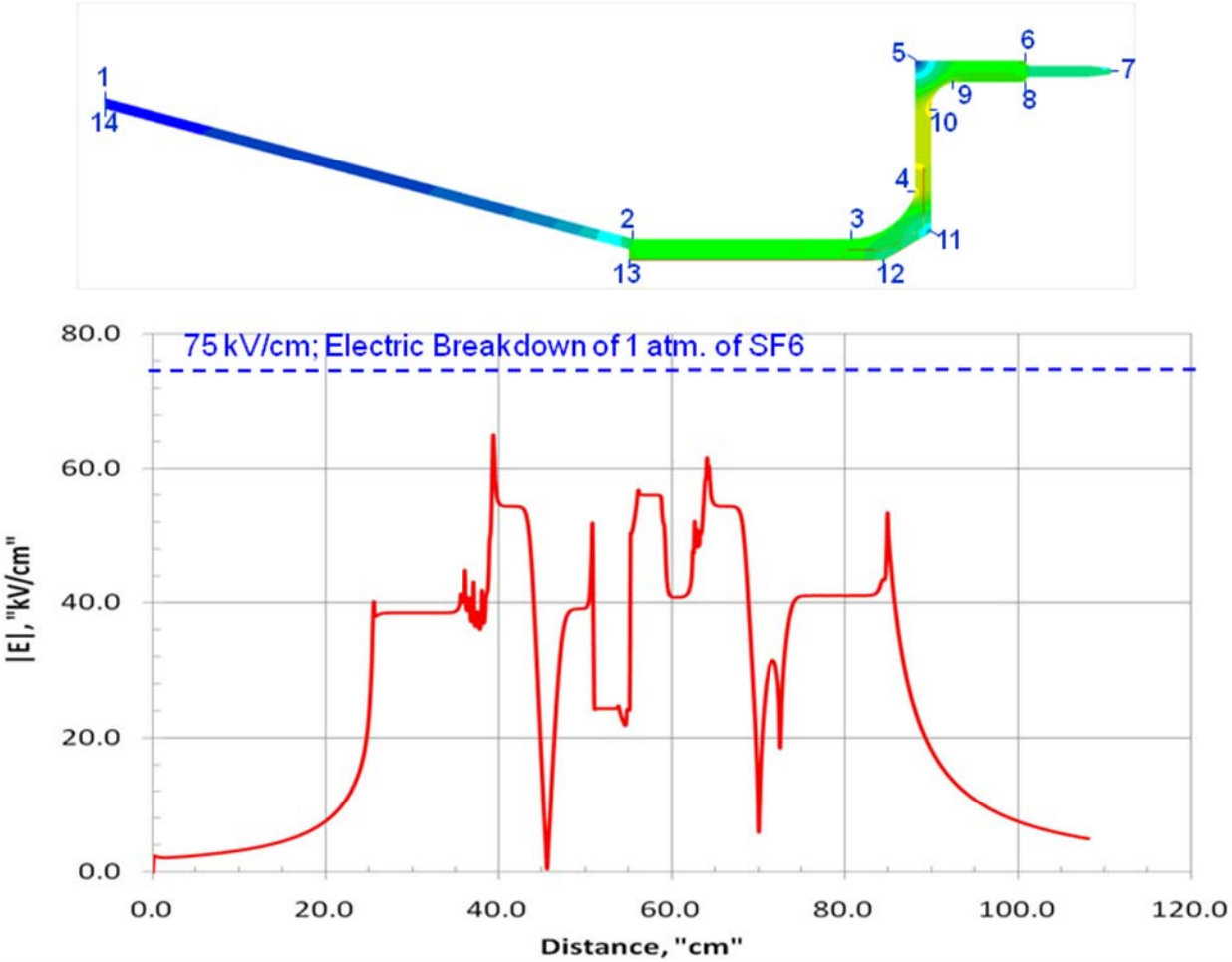
1
14
2
13
3
12
4
11
5
10
6
9
7
8
75 kV/cm; Electric Breakdown of 1 atm. of SF6
80.0
60.0
40.0
20.0
0.0
|E|, "kV/cm"
0.0
20.0
40.0
60.0
80.0
100.0
120.0
Distance, "cm"

Figure 14

Figure 15

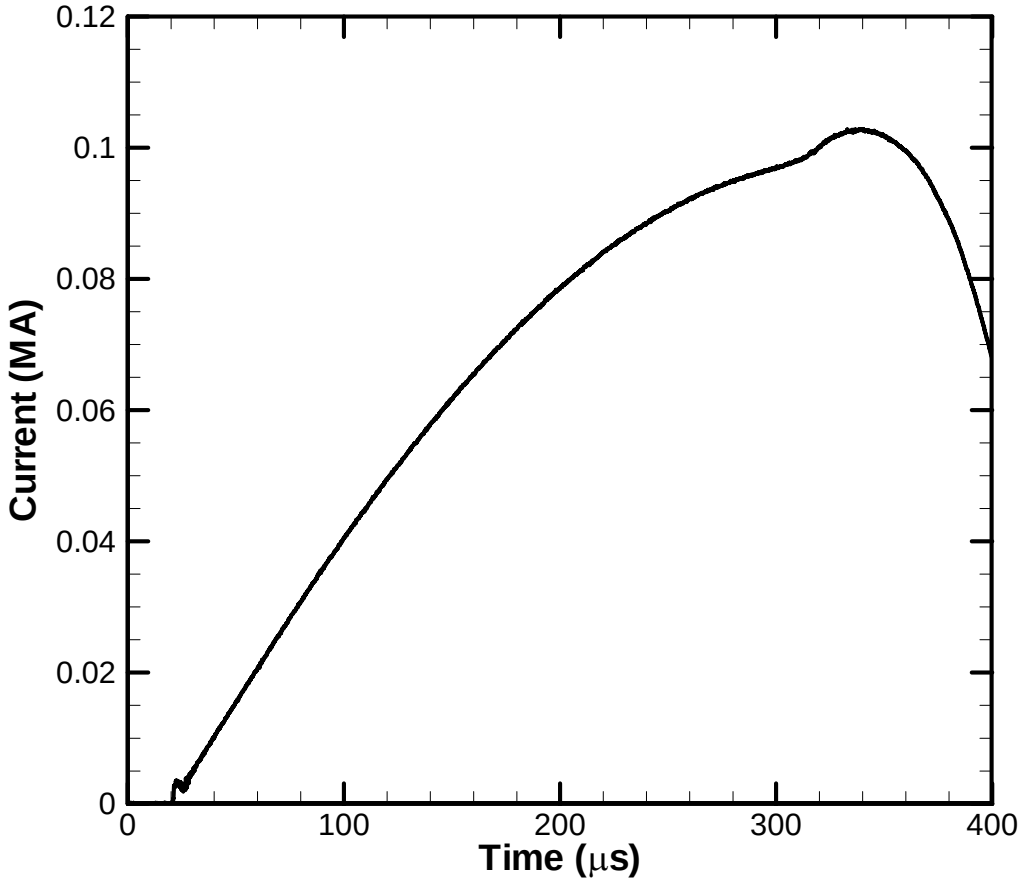

Figure 16

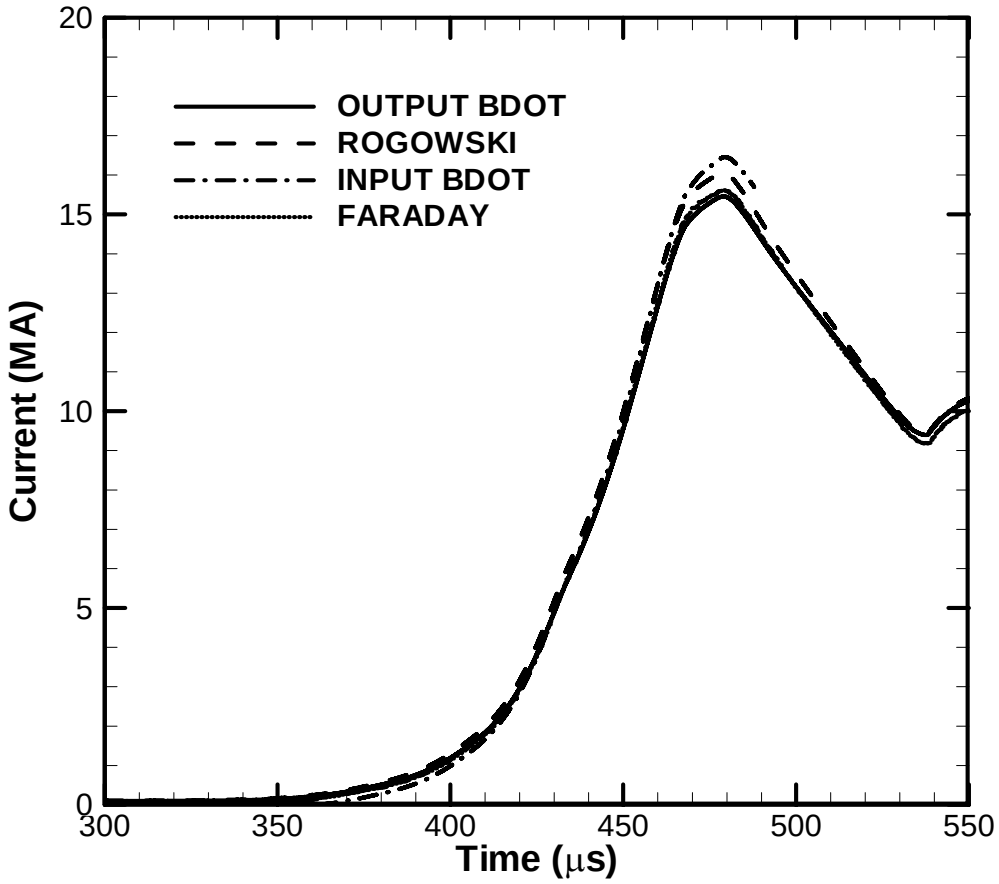
OUTPUT BDOT
ROGOWSKI
INPUT BDOT
FARADAY
Current (MA)
Time (μs)
0
5
10
15
20
300
350
400
450
500
550

Figure 17

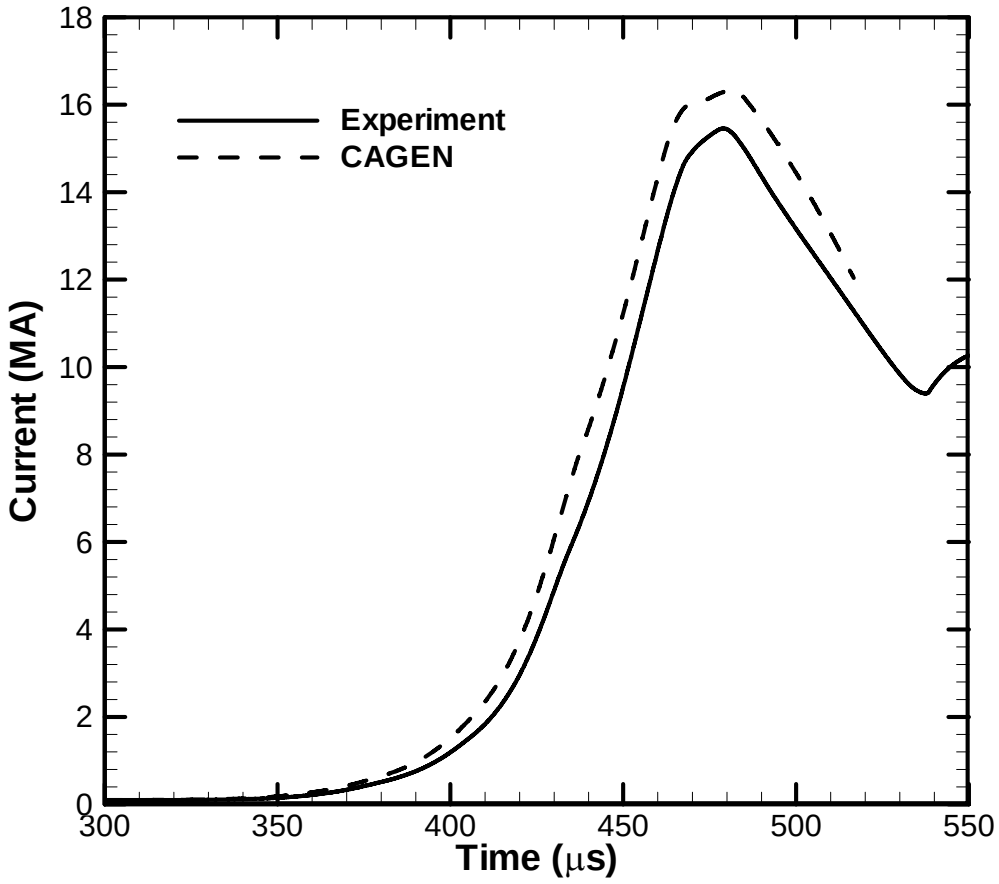
Experiment
CAGEN
Current (MA)
Time (μs)
0
2
4
6
8
10
12
14
16
18
300
350
400
450
500
550

Figure 18

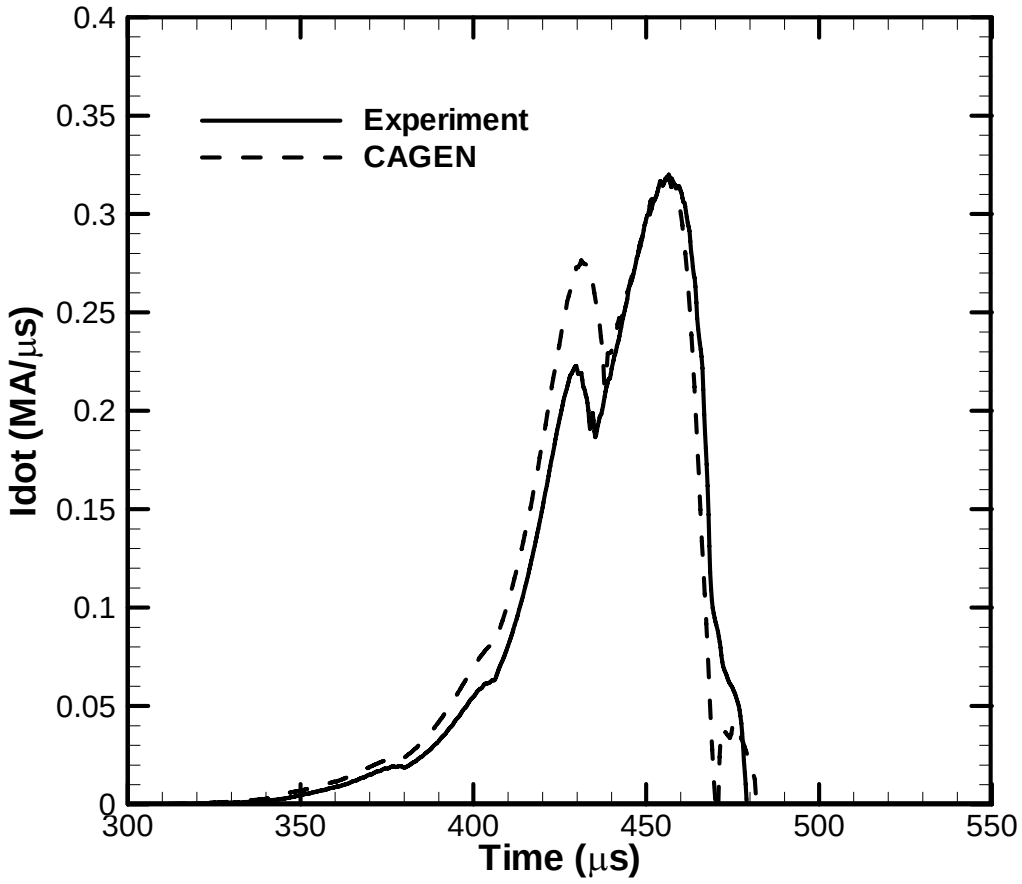
Experiment
CAGEN
Idot (MA/μs)
Time (μs)
0.4
0.35
0.3
0.25
0.2
0.15
0.1
0.05
0
300
350
400
450
500
550

Figure 19

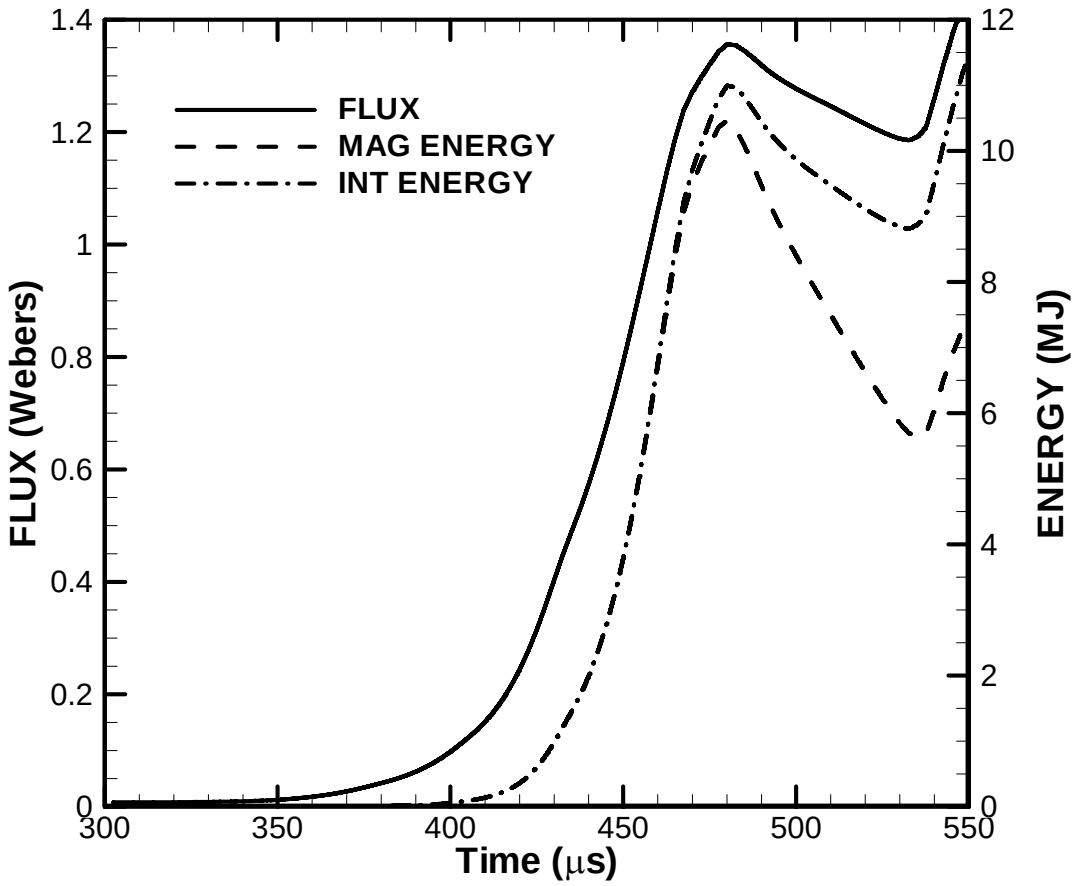
FLUX
MAG ENERGY
INT ENERGY
FLUX (Webers)
ENERGY (MJ)
Time (μs)
0
0.2
0.4
0.6
0.8
1
1.2
1.4
0
2
4
6
8
10
12
300
350
400
450
500
550

Figure 20

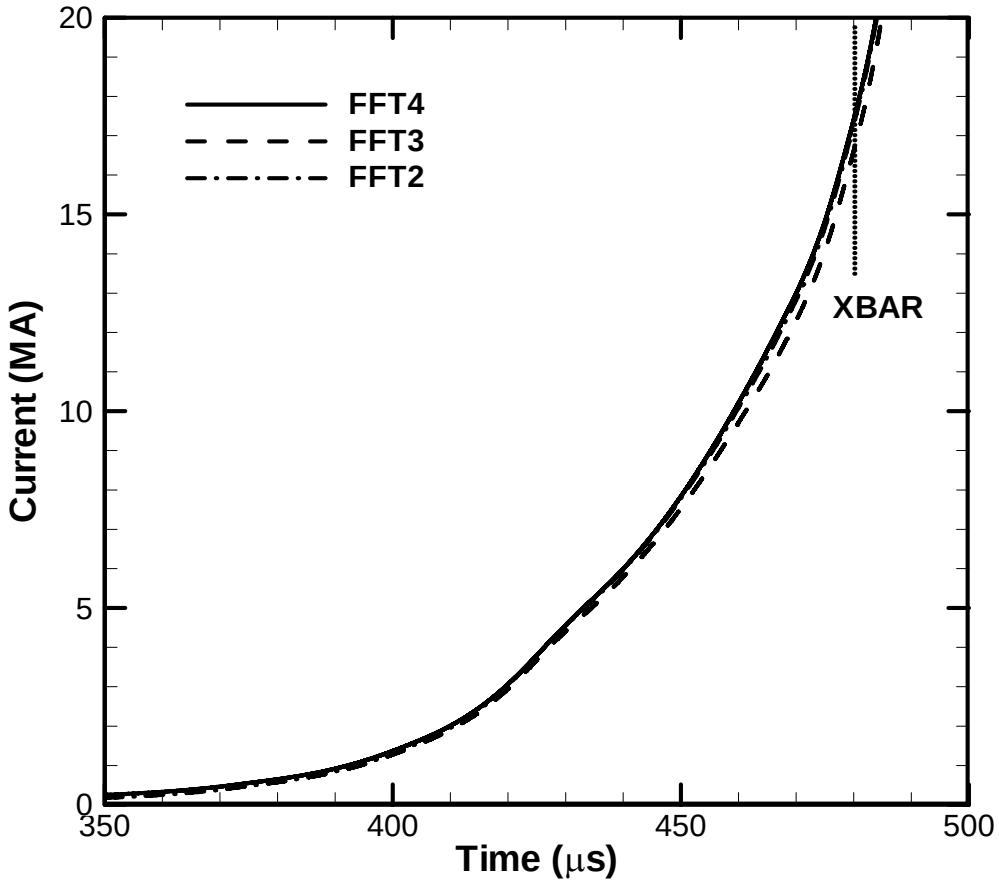
FFT4
FFT3
FFT2
XBAR
Current (MA)
Time (μs)
0
5
10
15
20
350
400
450
500

Figure 21